Universal Quantum Computation Based on Nanoscale Skyrmion Helicity Qubits in Frustrated Magnets

Jing Xia, Xichao Zhang, Xiaoxi Liu, Yan Zhou, and Motohiko Ezawa

Phys. Rev. Lett. **130**, 106701 — Published 7 March 2023

DOI: 10.1103/PhysRevLett.130.106701

Universal Quantum Computation Based on Nanoscale Skyrmion Helicity Qubits in Frustrated Magnets

Jing Xia,[1] Xichao Zhang,[1] Xiaoxi Liu,[1] Yan Zhou,[2,*] and Motohiko Ezawa[3,†]

[1]*Department of Electrical and Computer Engineering, Shinshu University, Wakasato 4-17-1, Nagano 380-8553, Japan*
[2]*School of Science and Engineering, The Chinese University of Hong Kong, Shenzhen, Guangdong 518172, China*
[3]*Department of Applied Physics, The University of Tokyo, 7-3-1 Hongo, Tokyo 113-8656, Japan*

(Dated: February 10, 2023)

We propose a skyrmion-based universal quantum computer. Skyrmions have the helicity degree of freedom in frustrated magnets, where two-fold degenerated Bloch-type skyrmions are energetically favored by the magnetic dipole-dipole interaction. We construct a qubit based on them. A skyrmion must become a quantum-mechanical object when its size is of the order of nanometers. It is shown that the universal quantum computation is possible based on nanoscale skyrmions in a magnetic bilayer system. The one-qubit quantum gates are materialized by controlling the electric field and the spin current. The two-qubit gate is materialized with the use of the Ising-type exchange coupling. The merit of the present mechanism is that external magnetic field is not necessary. Our results may open a possible way toward universal quantum computation based on nanoscale topological spin textures.

Introduction. The skyrmion is a classical topological soliton in a continuum theory. The magnetic skyrmion has attracted tremendous attention because it may be used for building spintronic applications [1–13] such as racetrack memory and logic gates [14–16]. It is a two-dimensional swirling spin texture in thin films. There is the helicity degree of freedom associated with the direction of the swirling in frustrated magnets. The energies of skyrmions are degenerate with respect to the helicity degree of freedom if the magnetic dipole-dipole interaction (DDI) is neglected [17–21]. Actually, the helicity is locked to two-fold degenerate Bloch-type skyrmions by the magnetic DDI [21, 22]. We also note that skyrmions in frustrated magnets with certain perpendicular magnetic anisotropy could be stabilized without applying external magnetic field [21, 23].

Although the skyrmion was initially introduced as a classical object, it must be a quantum object if the size of the skyrmion is of the order of nanometers [24–28]. Actually, skyrmions with atomic scale have been already experimentally manufactured in frustrated magnets [29–34], where the size is in the range of 3 nm - 10 nm. Most recently, it was proposed [24] that a skyrmion in a frustrated magnet can be used as a qubit based on the helicity degrees of freedom.

Quantum computation is expected to be the next-generation computation [35–37]. It is realized in various systems including superconductors [38], photonic systems [39], quantum dots [40], trapped ions [41], and nuclear magnetic resonance [42, 43]. Universal quantum computation is necessary for executing arbitrary quantum algorithm. The Solovay-Kitaev theorem dictates that only three quantum gates are enough for universal quantum computation [44–46]. They are the $\pi/4$ phase shift gate, the Hadamard gate, and the controlled-NOT (CNOT) gate, where the former two operators are one-qubit operators and the latter one is a two-qubit operator. In principle, one can perform an arbitrary rotation of the Bloch sphere based on these three quantum gates.

In this paper, we make the use of the two helicity states of a Bloch-type nanoscale skyrmion in frustrated magnets, where a linear combination of the two states is realized as a quantum-mechanical state. Then, we show that universal quantum computation is possible based on nanoscale skyrmion qubits by explicitly constructing the three necessary quantum gates. Our key observation is that the interlayer coupling between two skyrmions produces the Ising interaction. It is a basis of the CNOT gate. All qubit operations are executed by temporally controlling the electric field and the spin current. A merit of the present mechanism is that external magnetic field is not necessary. Furthermore, the present system consists of an array of skyrmions forming two chains in two layers, where the number of skyrmions can be large. Our results may open a way toward a skyrmion-based universal quantum computer.

Classical skyrmion in frustrated magnet. A skyrmion is a centrosymmetric swirling structure of spins, whose collective coordinates are the skyrmion center and the helicity η with $0 \leq \eta < 2\pi$. The spin texture located at the coordinate center is parametrized as

$$\boldsymbol{m}\,(x,y) = (\sin\theta(r)\cos\phi, \sin\theta(r)\sin\phi, \cos\theta(r)), \quad (1)$$

with

$$\phi = \varphi + \eta + \pi/2, \quad (2)$$

where φ is the azimuthal angle ($0 \leq \varphi < 2\pi$) satisfying $x = r\cos\varphi$, $y = r\sin\varphi$. We note that there is a difference from the conventional definition in Eq. (2) by the angle $\pi/2$.

There is a magnetic DDI in frustrated magnet. We have performed [21] a numerical analysis of the energy of a skyrmion parametrized by Eq. (1), and found that it depends on the helicity η as described by the effective Hamiltonian

$$H_V = -V\cos 2\eta, \quad (3)$$

where V denotes a certain positive constant depending on the magnitude of the magnetic DDI. We present the DDI energy

* Email: zhouyan@cuhk.edu.cn
† Email: ezawa@ap.t.u-tokyo.ac.jp

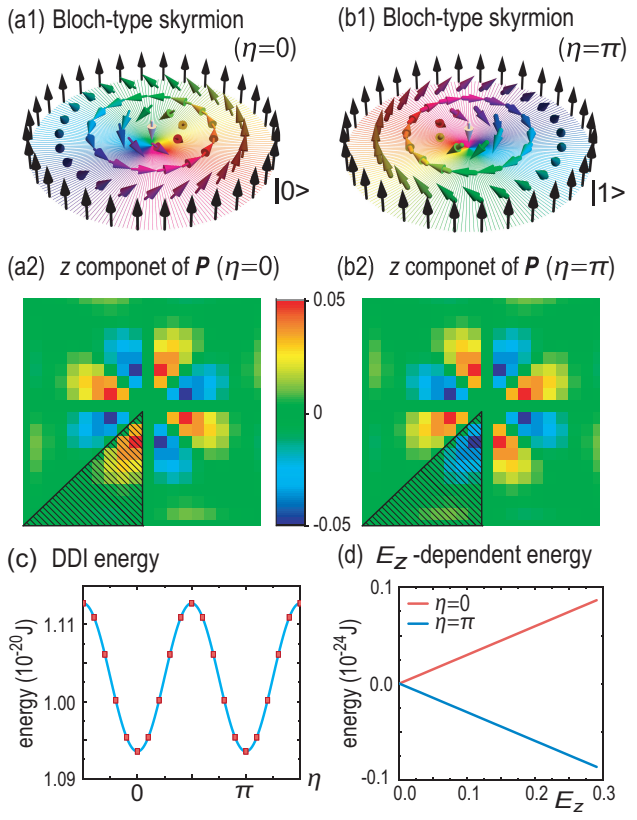

FIG. 1. (a1) and (b1) Illustration of Bloch-type skyrmions with the helicity (a1) $\eta = 0$ and (b1) π representing qubit states $|0\rangle$ and $|1\rangle$. The arrow represents the spin direction. The in-plane spin components are color coded by the rainbow color scheme. (a2) and (b2) Spatial profile of the electric polarization of the Bloch skyrmions. The color palette indicates the magnitude of the electric polarization in Eq.(5). (c) Helicity dependence of the energy due to the magnetic dipole-dipole interaction. (d) Electric field dependence of the energy. The horizontal axis is the applied electric field in units of mV/nm.

of a skyrmion evaluated newly in Fig. 1(c). See more details in Supplemental Materials I. Since the energy minimum is achieved at $\eta = 0$ and π, the helicity of a classical skyrmion is locked at $\eta = 0$ or π, as illustrated in Figs. 1(a1) and (b1). It is used as a classical bit $(|0\rangle, |1\rangle)$ corresponding to a pair of $\eta = 0$ and π, respectively.

When we apply a spin current, a helicity rotation occurs from $(|0\rangle, |1\rangle)$ to $(|1\rangle, |0\rangle)$. The effect is written in terms of the Pauli operator acting on the qubit basis

$$H_{J_{\text{current}}} = -\alpha_J J_{\text{current}} \left(|1\rangle\langle 0| + |0\rangle\langle 1|\right) = -\alpha_J J_{\text{current}} \sigma_x, \tag{4}$$

where α_J is a constant. Here we note that the current-induced switching of the helicity of a frustrated skyrmion has already been studied[21]. The required spin current J_{current} is of the order of 1 μA/nm^2, where the switching time is $\sim$100 [ps].

On the other hand, a noncollinear spin texture induces the electric dipole [47],

$$\boldsymbol{P}_{ij} = -\frac{Jea}{E_{\text{SO}}} \boldsymbol{e}_{ij} \times (\boldsymbol{S}_i \times \boldsymbol{S}_j), \tag{5}$$

where i and j are the site indices, $\boldsymbol{S}_i$ is the spin at the site i, $\boldsymbol{P}_{ij}$ is the electric dipole, $\boldsymbol{e}_{ij}$ is the unit vector pointing from the site i to the site j, J is the exchange coefficient, "a" is the distance between the neighboring magnetic ions, "e" is the electron charge and E_{SO} is the magnitude of the spin-orbit interactions. We have $Jea/E_{\text{SO}} = 4.86 \times 10^{29}$[Cm] with the use of $J = 10$[meV], $e = 1.62 \times 10^{-19}$[C], $a = 1$nm and $E_{\text{SO}} = 10$[meV].

The total electric polarization is given by the sum of the local electric dipole $\boldsymbol{P} = \sum_{\{i,j\}} \boldsymbol{P}_{ij}$. It is coupled to the electric field $\boldsymbol{E}$, where the Hamiltonian is given by $\boldsymbol{E} \cdot \boldsymbol{P}$. It is numerically estimated as $P = 0.598$. The energy of a spin texture under perpendicular electric field is estimated [48] by using $H_{E_z} = \boldsymbol{E} \cdot \boldsymbol{P}$, where $\boldsymbol{E} = (0, 0, E_z)$ is a perpendicular electric field and α_E is a constant.

With the use of the skyrmion configuration (1) for $\boldsymbol{S}_i$, we show the spatial distribution of electric dipole in Figs.1(a2) and (b2), which is calculated based on $\boldsymbol{P} = \sum_{\{i,j\}} \boldsymbol{P}_{ij}$ with Eq.(5). The electric dipole is opposite between the two Bloch skyrmions. For instance, we apply electric field locally in the shaded triangle as in Figs.1(a2) and (b2). The energy difference between the two helicities is found to increase linearly as a function of the applied electric field as in Fig.1(c). In terms of the helicity, this is written as

$$H_{E_z} = \alpha_E E_z \sigma_z, \tag{6}$$

because $\sigma_z(|0\rangle, |1\rangle)^t = (|0\rangle, -|1\rangle)^t$. We find from Fig.1(d) that the required electric field is of the order of 0.2 [mV/nm].

Helicity qubit. When the size of a skyrmion is of the order of nanoscale, it must become a quantum-mechanical object which can be a linear superposition of the two helicity states. Namely, the two Bloch-type states are lift up to form a qubit $(|0\rangle, |1\rangle)$. We discuss how to manipulate this qubit. On the other hand, we treat the position of the skyrmion center as a classical object which we can handle classically in this work. This is made possible by using an artificial pattern about which we discuss in a section named *pixelated skymion*.

Unitary gates. The dynamics of the helicity is governed by the Schrödinger equation

$$i\hbar \frac{d}{dt} |\psi\rangle = H |\psi\rangle, \tag{7}$$

where the single qubit Hamiltonian is given by

$$H = -\alpha_J J_{\text{current}} \sigma_x + \alpha_E E_z \sigma_z. \tag{8}$$

We solve Eq.(7) for a time-dependent J_{current} or E_z.

First, we set $J_{\text{current}} = 0$ and $\alpha_E E_z(t) = \hbar\theta/(2t_0)$ for $0 \le t \le t_0$ and $E_z(t) = 0$ otherwise. The solution of the Schrödinger equation reads

$$U_Z(\theta) = \exp\left[-\frac{i}{\hbar}\sigma_z \int_0^{t_0} \alpha_E E_z(t)\, dt\right] = \exp\left[-\frac{i\theta}{2}\sigma_z\right]. \tag{9}$$

This is the z-rotation gate by the angle θ.

Next, we set $E_z = 0$ and $\alpha_J J_{\text{current}}(t) = \hbar\theta/2t_0$ for $0 \le t \le t_0$ and $J_{\text{current}}(t) = 0$ otherwise. The solution of the Schrödinger equation reads

$$U_X(\theta) \equiv \exp\left[-(i\theta/2)\sigma_x\right]. \tag{10}$$

This is the x-rotation gate by the angle θ.

$\pi/4$ phase-shift gate. The $\pi/4$ phase-shift gate is realized by the z rotation (9) by the angle $-\pi/4$ as

$$U_T = e^{-i\pi/8} U_Z(\pi/4), \tag{11}$$

up to the overall phase factor $e^{-i\pi/8}$.

Hadamard gate. The Hadamard gate is realized by a sequential application of the z and x rotations [49] as

$$U_{\rm H} = -iU_Z(\pi/2)U_X(\pi/2)U_Z(\pi/2), \tag{12}$$

with the use of Eq. (9) and Eq. (10).

Multi-qubit gates. We have so far analyzed a single skyrmion for one-qubit gate operations. We now consider a magnetic bilayer system with an array of skyrmions made in such a way that no skyrmion is present above or below a skyrmion as in Fig. 2(a), where the number m is assigned to each skyrmion. Let the system contain N skyrmions in total, where N can be very large in principle.

The m-th skyrmion presents the m-th qubit. In general, multi qubits are given by $|s_1 s_2 \cdots s_N\rangle = |s_1\rangle_1 |s_2\rangle_2 \cdots |s_N\rangle_N$, where $|s_i\rangle_m$ denotes the m-th qubit and $s_i = 0, 1$.

Initially, all skyrmions are away from each other, and there is no interaction between them. When two skyrmions in the top and bottom layers approach one to another as shown in Fig. 2(c), the exchange interaction begins to operate between them. The interlayer coupling of the helicity is described by the XY model,

$$H_{\rm inter}(d_m) = -J_{\rm int}(d_m)(S_x^{(m)} S_x^{(m+1)} + S_y^{(m)} S_y^{(m+1)}), \tag{13}$$

because $S_z^{(m)} = 0$, where d_m represents the horizontal distance between these two skyrmion centers.

Inserting Eq. (1) into this equation with $\theta = \pi/2$, we obtain

$$H_{\rm inter}^m(d_m) \equiv -J_{\rm int}(d_m)\cos(\eta_m - \eta_{m+1}). \tag{14}$$

This exchange interaction is rewritten in the form of the Ising interaction,

$$H_{\rm Ising}^m(d_m) = -J_{\rm int}(d_m)\sigma_z^{(m)}\sigma_z^{(m+1)}. \tag{15}$$

The equivalence between Eqs. (14) and (15) is shown by acting them on the 2 qubits made of the m-th skyrmion and the (m+1)-th skyrmion.

As mentioned above, the position of the skyrmion center is treated as a classical object, which we can control externally. We manually control d_m as a function of time. Then, the time evolution is given by

$$U = \exp\left[-\frac{i}{\hbar}\int_0^{t_0} H_{\rm Ising}^m(d_m(t))\,dt\right] \tag{16}$$

with $d_m = d_m(t)$ in Eq. (15). If we set

$$J_{\rm int}(d_m(t)) = \hbar\theta/2t_0 \tag{17}$$

for $0 \le t \le t_0$ and $J_{\rm int}(d_m(t)) = 0$ otherwise, we obtain the Ising coupling gate

$$U_{ZZ}^{(m)}(\theta) \equiv \exp[-i(\theta/2)\sigma_z^{(m)}\sigma_z^{(m+1)}], \tag{18}$$

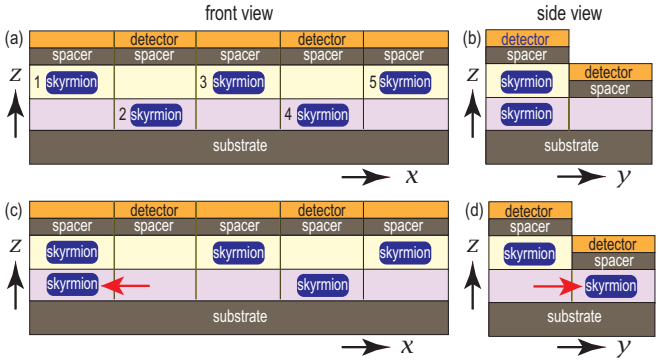

FIG. 2. Schematic illustrations of (a) the front view and (b) side view of an array of skyrmions in a magnetic bilayer system for quantum computing. We have numbered the skyrmion by the index m in (a). (c) Schematic illustration of the front view showing that a skyrmion is moved to the neighboring position for the Ising gate operation. (d) Schematic illustration of the side view showing that skyrmions in the bottom layer are driven to the readout positions.

acting on the 2 qubits.

We numerically estimate the exchange coupling $J_{\rm int}(0)$, which is the energy difference between the identical and opposite helicities, as $J_{\rm int}(0) \sim 4.7 \times 10^{-22}$[J]. The operating time is ∼0.18 [ps], which is estimated based on (17). Details are given in Supplemental Materials II.

CZ gate. The CZ gate is constructed based on the Ising interaction, which is given by [50]

$$U_{\rm CZ} = e^{i\pi/4} U_Z^{(1)}(\pi/2) U_Z^{(2)}(\pi/2) U_{ZZ}(-\pi/2), \tag{19}$$

where $U_Z^{(1)}$ ($U_Z^{(2)}$) is the Pauli-Z gate acting on the first (second) qubit. See Supplemental Material III for details.

CNOT gate. The CNOT gate is constructed by a sequential application of the CZ gate and the Hadamard gate

$$U_{\rm CNOT}^{1\to 2} = U_{\rm H}^{(2)} U_{\rm CZ} U_{\rm H}^{(2)}, \tag{20}$$

where $U_{\rm H}^{(2)}$ is the Hadamard gate acting on the second qubit. See Supplemental Material III for details.

Initialization. In order to execute quantum computation, we need to prepare an initial state $|00\cdots0\rangle$. We apply electric field E_z to all skyrmions, which resolves the degeneracy between the two Bloch-type skyrmions in each layer so that the state $|0\rangle$ has the lower energy. By cooling down the sample, each qubit falls into the ground state $|0\rangle$. Hence, after switching off the electric field, the system is initialized as $|00\cdots0\rangle$.

Readout process. The bilayer system has a step-like structures as in Fig. 2(b), and a tunnel magnetoresistance detector placed upon each magnetic layer can read out the helicity of the skyrmion underneath the detector [51]. After quantum computation is over, the helicity of a skyrmions in the top layer can be read out directly. With respect to the skyrmions in the bottom layer, a current is applied to drive the skyrmions toward the right side of the system as in Fig. 2(d), and then the helicity is read out.

The helicity of a skyrmion could also be observed by using the Lorentz transmission electron microscopy technique [12],

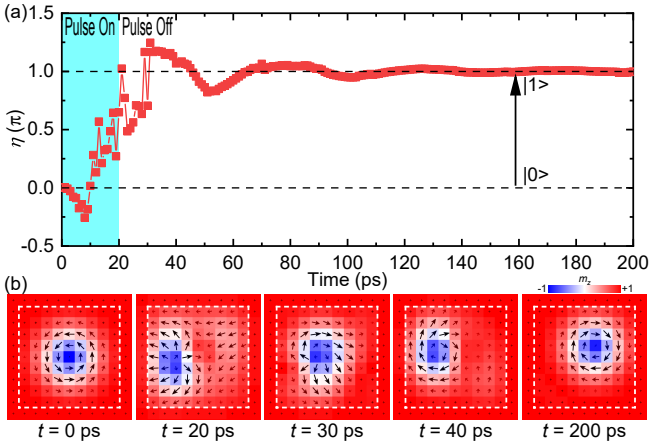

FIG. 3. Current-induced helicity flipping of a frustrated skyrmion confined in a square pinning pattern. (a) The helicity of the skyrmion as a function of time. The current pulse $j = 70$ MAcm^{-2} is applied for $t = 0 - 20$ ps, followed by a relaxation of 180 ps. A relaxed skyrmion with $\eta = 0$ is initially placed at the center of a sample with 19×19 spins. The skyrmion helicity is flipped to $\eta = \pi$ after the pulse injection. The lattice constant is $a = 0.4$ nm. The parameters are adopted from Ref.[21]. (b) Selected top-view snapshots showing the flipping of the skyrmion helicity. We have set the enhanced anisotropy $K_{\rm p} = 1$ in the area outside the dotted white square, where spins are pinned upward.

the nitrogen-vacancy (NV) magnetometry [52] and the resonant elastic x-ray scattering [53] combined with the FM resonance measurements [54].

By observing the helicity, it is fixed either at $\eta = 0$ or π because they are two-fold degenerate ground states. The result is $|s_1 s_2 \cdots s_N\rangle$. This is a standard representation of the readout process of quantum computation.

Pixelated skyrmion. In the present proposal, it is necessary to control precisely the position of a skyrmion to make an array of skyrmions as in Fig. 2(a). A precise control is also necessary to execute the Ising gate operation. A recent theoretical report has suggested that the position of a nanoscale skyrmion could be digitalized by introducing a square-grid pinning pattern in a thin-film sample hosting a skyrmion [55]. To be specific, one can fabricate a sample where the easy-axis magnetic anisotropy is modulated with a grid-pattern landscape. A skyrmion is trapped to this grid and thus its center is digitalized. Although this architecture was proposed for nanoscale skyrmions in ferromagnets with Dzyaloshinskii-Moriya interaction [55], it would also be possible to apply it to the system of nanoscale skyrmions in frustrated magnets. Then, the center of the skyrmion is digitalized, as makes a precise control of a skyrmion possible. The flipping process of the helicity in a frustrated magnet with an appropriately patterned grid is shown in Fig.3.

Finite temperature effects. The helicity of the nanoscale frustrated skyrmion is switched by thermal effect. In Supplemental Material IV, we numerically demonstrate based on the stochastic LLG equation[56] that the switching of the helicity of a frustrated skyrmion between $\eta = 0$ and $\eta = \pi$ is induced by thermal fluctuations when the temperature is above 3.8K.

Discussions. We comment on the relevance to a recent theoretical report [24] on qubits based on skyrmions. First, although both the mechanisms use the helicity of a skyrmion as a qubit, its dynamical origin is quite different. Indeed, the magnetic DDI plays an essential role in the present work but is neglected in the previous report. We have used the fact that the magnetic DDI term favors two different configurations of Bloch-type skyrmions in frustrated magnets. Second, we have argued how to perform universal quantum computation, but this is not the case in the previous proposal. Third, the mechanism of the helicity control is quite different. In controlling qubits, electric fields and spin currents are used in our proposal, while external magnetic fields are used in the previous proposal. The merit of our method is that it is easier to control locally electric fields and spin currents than magnetic fields. Furthermore, the present system is scalable to the large number of qubits, since it consists of an array of skyrmions forming two chains in a magnetic bilayer, where the number of skyrmions can be as large as possible.

The Bloch-type nanoscale skyrmion state has been found in the frustrated centrosymmetric triangular-lattice magnet Gd_2PdSi_3 at low temperatures[22]. Other candidate materials for hosting frustrated skyrmions would be triangular magnets with transition mental ions[17], such as $NiGa_2S_4$[57] [58], α-NaFeO2[59] and dihalides $Fe_xNi_{1-x}Br_2$[60]. Besides, $Pb_2VO(PO_4)_2$ has a frustrated square lattice with ferromagnetic nearest-neighbor interaction in the new compound[61]. Most theoretical works on frustrated skyrmions are based on a single layer or bulk of ferromagnet with exchange frustrations. Our theoretical proposal will motivate experimentalists to manufacture a bilayer system based on frustrated magnets. For example, one may be able to use frustrated van der Waals ferromagnets to construct a bilayer structure hosting skyrmions [62].

M.E. is very much grateful to N. Nagaosa for helpful discussions on the subject. This work is supported by the Grants-in-Aid for Scientific Research from MEXT KAKENHI (Grants No. JP18H03676). This work is also supported by CREST, JST (Grants No. JPMJCR20T2). J.X. was a JSPS International Research Fellow supported by JSPS KAKENHI (Grant No. JP22F22061). X.L. acknowledges support by the Grants-in-Aid for Scientific Research from JSPS KAKENHI (Grant Nos. JP20F20363, JP21H01364, JP21K18872, and JP22F22061). Y.Z. acknowledges support by Guangdong Basic and Applied Basic Research Foundation (2021B1515120047), Guangdong Special Support Project (Grant No. 2019BT02X030), Shenzhen Fundamental Research Fund (Grant No. JCYJ20210324120213037), Shenzhen Peacock Group Plan (Grant No. KQTD20180413181702403), Pearl River Recruitment Program of Talents (Grant No. 2017GC010293), and National Natural Science Foundation of China (Grant Nos. 11974298, 12004320, and 61961136006).

[1] N. Nagaosa and Y. Tokura, Nat. Nanotech. **8**, 899 (2013).
[2] M.Mochizuki and S. Seki, J. Phys.: Condens. Matter **27**, 503001 (2015).
[3] G. Finocchio, F. Büttner, R. Tomasello, M. Carpentieri, and M. Kläui, J. Phys. D: Appl. Phys. **49**, 423001 (2016).
[4] R. Wiesendanger, Nat. Rev. Mat. **1**, 16044 (2016).
[5] A. Fert, N. Reyren, and V. Cros, Nat. Rev. Mater. **2**, 17031 (2017).
[6] X. Zhang, Y. Zhou, K. M. Song, T.-E. Park, J. Xia, M. Ezawa, X. Liu, W. Zhao, G. Zhao, and S. Woo, J. Phys. Condens. Matter **32**, 143001 (2020).
[7] B. Göbel, I. Mertig, and O. A. Tretiakov, Phys. Rep. **895**, 1 (2021).
[8] C. Reichhardt, C. J. O. Reichhardt, and M. V. Milosevic, Rev. Mod. Phys. 94, 035005 (2022).
[9] Y. Zhou, Natl. Sci. Rev. **6**, 210 (2019).
[10] S. Li, W. Kang, X. Zhang, T. Nie, Y. Zhou, K. L. Wang, and W. Zhao, Mater. Horiz. **8**, 854, (2021).
[11] Y. Tokura and N. Kanazawa, Chem. Rev. **121**, 2857 (2021).
[12] X. Yu, J. Magn. Magn. Mater **539**, 168332 (2021).
[13] C. H. Marrows and K. Zeissler, Appl. Phys. Lett. **119**, 250502 (2021).
[14] J. Sampaio, V. Cros, S. Rohart, A. Thiaville, and A. Fert, Nat. Nanotechnol. **8**, 839 (2013).
[15] R. Tomasello, E. Martinez, R. Zivieri, L. Torres, M. Carpentieri, and G. Finocchio, Sci. Rep. **4**, 6784 (2014).
[16] X. Zhang, M. Ezawa, and Y. Zhou, Sci. Rep. **5**, 9400 (2015).
[17] A. O. Leonov and M. Mostovoy, Nat. Commun. **6**, 8275 (2015).
[18] S.-Z. Lin and S. Hayami, Phys. Rev. B **93**, 064430 (2016).
[19] C. D. Batista, S.-Z. Lin, S. Hayami, and Y. Kamiya, Rep. Prog. Phys. **79**, 084504 (2016).
[20] H. T. Diep, Entropy **21**, 175 (2019).
[21] X. Zhang, J. Xia, Y. Zhou, X. Liu, H. Zhang, M. Ezawa, Nat. Com. **8**, 1717 (2017).
[22] T. Kurumaji, T. Nakajima, M. Hirschberger, A. Kikkawa, Y. Yamasaki, H. Sagayama, H. Nakao, Y. Taguchi, T.-H. Arima, and Y. Tokura, Science **365**, 914 (2019).
[23] J. Xia, X. Zhang, M. Ezawa, O. A. Tretiakov, Z. Hou, W. Wang, G. Zhao, X. Liu, H. T. Diep, and Y. Zhou, Appl. Phys. Lett. **117**, 012403 (2020)
[24] C. Psaroudaki and C. Panagopoulos, Phys. Rev. Lett. **127**, 067201 (2021).
[25] V. Lohani, C. Hickey, J. Masell, and A. Rosch, Phys. Rev. X **9**, 041063 (2019).
[26] P. Siegl, E. Y. Vedmedenko, M. Stier, M. Thorwart, and T. Posske, Phys. Rev. Research 4, 023111, (2022).
[27] A. Haller, S. Groenendijk, A. Habibi, A. Michels, and T. L. Schmidt, Phys. Rev. Research 4, 043113 (2022)
[28] K. Mæland and A. Sudbø, Phys. Rev. B 105, 224416 (2022).
[29] S. Heinze, K. von Bergmann, M. Menzel, J. Brede, A. Kubetzka, R. Wiesendanger, G. Bihlmayer and S. Blugel, Nature Physics **7**, 713 (2011).
[30] A. Schlenhoff, P. Lindner, J. Friedlein, S. Krause, R. Wiesendanger, M. Weinl, M. Schreck and M. Albrecht, ACS Nano 9, 5908 (2015).
[31] A. Roldan-Molina, A. S. Nunez and J. Fernandez-Rossie, New J. Phys. **18**, 045015(2016).
[32] J. Grenz, A. Kohler, A. Schwarz and R. Wiesendanger, Phys. Rev. Lett. **119**, 047205 (2017).
[33] N. Swain, M. Shahzad and P. Sengupta, arXiv:2203.03359.
[34] R. Bruning, A. Kubetzka, K. von Bergmann, E. Y. Vedmedenko, R. Wiesendanger, Phys. Rev. B 105, L241401 (2022)
[35] R. Feynman, Int. J. Theor. Phys. **21**, 467 (1982).
[36] D. P. DiVincenzo, Science **270**, 255 (1995).
[37] M. Nielsen and I. Chuang, "Quantum Computation and Quantum Information", Cambridge University Press, (2016); ISBN 978-1-107-00217-3.
[38] Y. Nakamura; Yu. A. Pashkin; J. S. Tsai, Nature **398**, 786 (1999).
[39] E. Knill, R. Laflamme and G. J. Milburn, Nature, **409**, 46 (2001).
[40] D. Loss and D. P. DiVincenzo, Phys. Rev. A **57**, 120 (1998).
[41] J. I. Cirac and P. Zoller, Phys. Rev. Lett. **74**, 4091 (1995).
[42] L. M.K. Vandersypen, M. Steffen, G. Breyta, C. S. Yannoni, M. H. Sherwood, I. L. Chuang, Nature **414**, 883 (2001).
[43] B. E. Kane, Nature **393**, 133 (1998).
[44] D. Deutsch, Proceedings of the Royal Society A. **400**, 97 (1985).
[45] C. M. Dawson and M. A. Nielsen, Quantum Information and Computation **6**, 81 (2006).
[46] M. Nielsen and I. Chuang, "Quantum Computation and Quantum Information", Cambridge University Press, Cambridge, UK (2010).
[47] H. Katsura, N. Nagaosa and A. V. Balatsky, Phys. Rev. Lett. **95**, 057205 (2005).
[48] X. Yao, J. Chen and S. Dong, New J. Phys. **22**, 083032 (2020).
[49] N. Schuch and J. Seiwert, Phys. Rev. A **67**, 032301 (2003).
[50] Y. Makhlin, Quant. Info. Proc. **1**, 243 (2002).
[51] H. Chen, W. Bouckaert, S. A. Majetich, J. Magn. Magn. Mater **541**, 168552 (2022).
[52] Y. Dovzhenko, F. Casola, S. Schlotter, T. X. Zhou, F. Buttner, R. L. Walsworth, G. S. D. Beach, and A. Yacoby, Nat. Commun. **9**, 2712 (2018).
[53] S. L. Zhang, G. van der Laan, W. W. Wang, A. A. Haghighirad, and T. Hesjedal, Phys. Rev. Lett. **120**, 227202 (2018).
[54] S. Pöllath, A. Aqeel, A. Bauer, C. Luo, H. Ryll, F. Radu, C. Pfleiderer, G. Woltersdorf, and C. H. Back, Phys. Rev. Lett. **123**, 167201 (2019).
[55] X. Zhang, J. Xia, K. Shirai, H. Fujiwara, O. A. Tretiakov, M. Ezawa, Y. Zhou, X. Liu, Com. Phys. **4**, 255 (2021).
[56] J. Barker and O. A. Tretiakov, *Phys. Rev. Lett.* **116**, 147203 (2016).
[57] S. Nakatsuji, Y. Nambu H. Tonomura, O. Sakai, S. Jonas, C. Broholm, H. Tsunetsugu, Y. Qiuand, Y. Maeno, Science **9**, 1697 (2005)
[58] C. Stock, S. Jonas, C. Broholm, S. Nakatsuji, Y. Nambu, K. Onuma, Y. Maeno, and J.-H. Chung Phys. Rev. Lett. **105**, 037402 (2010)
[59] T. McQueen, Q. Huang, J. W. Lynn, R. F. Berger, T. Klimczuk, B. G. Ueland, P. Schiffer, and R. J. Cava Phys. Rev. B **76**, 024420 (2007)
[60] L. P. Regnault, J. Rossat-Mignod, A. Adam, D. Billerey and C. Terrier, J. Phys. France **43**, 1283 (1982)
[61] E.E.Kaula, H.Rosnera, N.Shannonb, R.V.Shpanchenkoc and C.Geibela, J. Mag. Mag. Mat. **272**, 922 (2004)
[62] A. M. Ukpong, Nanomaterials **11**, 1770 (2021).